Chromatic Dispersion Compensation Using Full-Field Maximum Likelihood Sequence Estimation

Jian Zhao, Mary E. McCarthy, Andrew D. Ellis and Paul Gunning

Abstract— **We investigate full-field detection based maximum likelihood sequence estimation (MLSE) for chromatic dispersion compensation in 10Gbit/s on-off keyed optical communication systems. Important design criteria are identified to optimize the system performance. It is confirmed that approximately 50% improvement in transmission reach can be achieved compared to conventional direct-detection MLSE at both 4 and 16 states. It is also shown that full-field MLSE is more robust to the noise and the associated noise amplifications in full-field reconstruction, and consequently exhibits better tolerance to non-optimized system parameters than full-field feed-forward equalizer. Experiments over 124km spans of field-installed single-mode fibre without optical dispersion compensation using full-field MLSE verify the theoretically predicted performance benefits.**

Index Terms— **Modulation, Chromatic Dispersion, Electronic Dispersion Compensation, Detection**

I. Introduction

MAXIMUM likelihood sequence estimation (MLSE) is an optimum receiver in linear communication systems [1], and has attracted much interest recently when applied to chromatic dispersion (CD) compensation in optical communications [2-5]. Recent advances in high speed microelectronics, including 30Gsamples/s analogue-to-digital converters (ADCs), have made its use in 10Gbit/s systems practical [6]. A direct-detection MLSE (DD MLSE) receiver is commercially available and was demonstrated in various transmission experiments [7-9]. However, direct detection (a form of square law detection) results in the transformation of CD from a linear impairment in the optical domain to a nonlinear impairment in the electrical domain, destroying the fundamental condition that MLSE requires for optimum operation. Consequently, the system performance is unavoidably limited by the loss of signal phase information.

Manuscript received August 3, 2009. This work was supported by Science Foundation Ireland 06/IN/I969 and Enterprise Ireland CFTD/08/333.

Jian Zhao, Mary E. McCarthy, and Andrew D. Ellis are with Photonic Systems Group, Tyndall National Institute and Department of Physics, University College Cork, Lee Maltings, Prospect Row, Cork, Ireland (e-mail: jian.zhao@tyndall.ie).

P. Gunning is with Futures Testbed, BT Design, Martlesham Heath, Ipswich, UK.

This performance limitation could be removed by restoring channel linearity using coherent detection [10-11] or direct-detection based full-field reconstruction [12-15]. The first method achieves optimum performance theoretically, but requires additional tight-specification optical components, and signal polarization and phase recovery. In contrast, the second technique, by extracting the intensity and instantaneous frequency information simultaneously using a single asymmetric Mach-Zehnder interferometer (AMZI) and two photodiodes, loosens the specifications and is a more cost-effective approach. This technique has been experimentally verified to recover a 10Gbit/s on-off keyed (OOK) signal after transmission through 372km of field-installed single-mode fibre (SMF) using 4-state full-field MLSE [13,15].

In this paper, we will extend our earlier report to a more systematic investigation for both 4- and 16-state full-field MLSE. We will theoretically identify the design criteria to optimize the system performance and confirm its advantages in the performance limit (under optimized parameters) compared to conventional DD MLSE. We will also show that full-field MLSE exhibits better tolerance to the noise and the associated noise amplification mechanisms in full-field reconstruction when compared to other full-field electronic dispersion compensation (EDC) methods including feed-forward equalizer (FFE). Experimental investigations extending the transmission reach to 496km field-installed SMF were undertaken and showed close agreement with the theory. The paper is organised as follows: we will present the principle of full-field MLSE in Section II and systematically investigate the performance and design criteria by simulations in Section III. Experiments that verify the theoretically predicted performance benefits are described in Section IV. Finally, Section V summarizes the results.

II. Principle

Fig. 1 depicts the principle of full-field MLSE. The incoming optical signal is processed by a single AMZI with a differential time delay (DTD) of Δt and differential phase shift of $\pi/2$. Assuming that the input optical field (baseband representation) is, $|E(t)|\exp(j\int_{-\infty}^{t}\Delta\omega(\tau)d\tau)$ where $\Delta\omega(\tau)$ $(=\omega(\tau)-\omega_0)$ is the instantaneous frequency of baseband representation of the optical field, signals proportional to the amplitude and

instantaneous frequency of the optical field, $V_A(t)$ and $V_f(t)$, can be extracted by mathematical manipulation [14]:

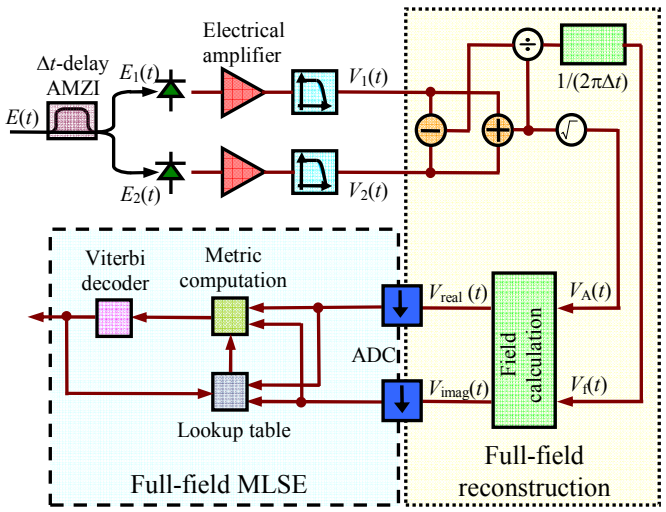

Fig. 1. Principle of full-field MLSE

$$V_A(t) = [V_1(t) + V_2(t)]^{1/2} = |E(t)|$$

$$V_f(t) = [V_1(t) - V_2(t)]/[2\pi\Delta t V_1(t) + 2\pi\Delta t V_2(t)] \approx \Delta\omega(t)/2\pi \quad (1)$$

where "≈" is used because $\sin(\Delta\omega(t)\Delta t)/(2\pi\Delta t)$ is approximated as $\Delta\omega(t)/2\pi$ in the derivation [14]. This assumption is valid given $\Delta\omega(t)\Delta t<<1$. The intensity and frequency information is exploited to reconstruct the full optical field consisting of the in-phase and quadrature components. The full-field reconstruction module (in dotted box) may be implemented using analogue [12] or digital devices. In the latter case, ADCs are used to sample and quantize $V_1(t)$ and $V_2(t)$. Several additional signal processing components, not shown in Fig. 1 but described in the following sections, serve to improve the quality of the phase estimation and to overcome the susceptibility to noise and associated noise amplification mechanisms during the full-field reconstruction process. We attribute this susceptibility to two main mechanisms: Firstly, the received value of $V_A(t)$ for a sequence of consecutive logical data '0's is small such that any noise leads to large estimation inaccuracy in $V_f(t)=(V_1(t)-V_2(t))/[2\pi\Delta t \cdot V_A(t)^2]$. Secondly, the low-frequency contents of the noise and the inaccuracy in the estimated frequency, $V_f(t)$, are increased by a low-frequency component amplification mechanism [14].

The recovered optical field, after sampling and ADCs, allows for CD compensation using full-field MLSE, which, differing from DD MLSE, exploits the real and imaginary information simultaneously for both metric computation and channel training. The metric of full-field MLSE, $PM(b_n)$, is:

$$PM(b_n) = PM(b_{n-1}) - \sum_i \log(p(I_{real}(t_i), I_{imag}(t_i) \mid b_{n-m},...,b_n)) \quad (2)$$

where $i \in \{n\ n+1/2\}$ for two samples per bit assumed in this paper. b_n and $p(I_{real}(t_i), I_{imag}(t_i) \mid b_{n-m},\ldots,b_n)$ are the n^{th} OOK logical data and the two-dimensional joint probability of the full optical field at time t_i given the logical data $b_{n-m},\ldots,b_n$, respectively. m is the memory length. In this paper, the initial metrics are obtained using the nonparametric histogram method [4]. The required lookup table size for $p(I_{real}(t_i), I_{imag}(t_i)|b_{n-m},\ldots,b_n)$ is proportional to 2^{2q+m+2} at two samples per bit, when q is the ADC resolution. The complexities of the metric computation and the Viterbi decoding are the same as those of a DD MLSE with the same state number, and are proportional to 2^{m+1} and 2^m respectively. In addition to the full expression of metric (2), another reduced metric is also investigated, which approximates (2) with greatly reduced lookup table complexity:

$$PM(b_n) = PM(b_{n-1}) - \sum_i \log(p(I_{real}(t_i) \mid b_{n-m},...,b_n) \cdot p(I_{imag}(t_i) \mid b_{n-m},...,b_n)) \quad (3)$$

In (3), it is assumed that the probability distributions for the real and imaginary signals are independent. This simplification, as will be shown later, compared to the full metric (2), causes only a slight performance penalty when used with optimized system parameters, while significantly reducing the memory size and the time required for lookup table setup and update from 2^{2q+m+2} to 2^{q+m+3}.

III. Numerical Investigation

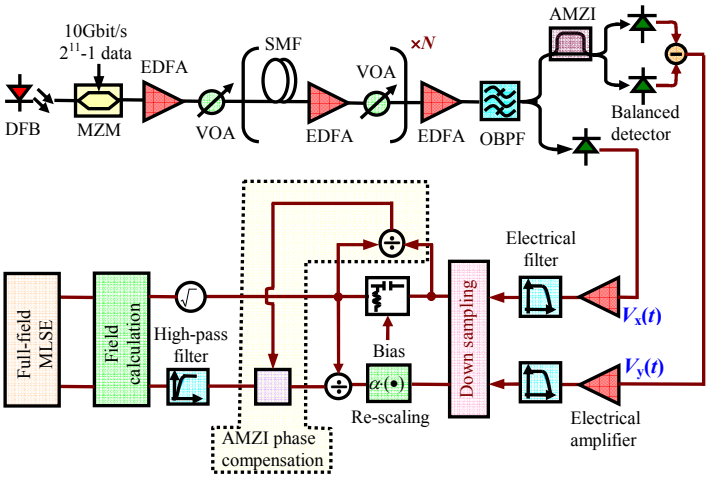

Fig. 2. Simulation model

Fig. 1 shows the operating principle. However, it is difficult in practice to precisely match the responses of two independent receiver chains. Therefore, we adopted an equivalent implementation using a balanced photo-detector to give V_1-V_2 and an additional single photo-detector to obtain V_1+V_2 [12-13]. Fig. 2 represents the simulation model used in this paper. It was implemented using Matlab codes. Continuous wave light was intensity modulated by a 10Gbit/s OOK data train using a Mach-Zehnder modulator (MZM). The data train consisted of a 2^{11}-1 pseudo-random binary sequence (PRBS) repeated nine times (18,423 bits). Ten '0' bits and eleven '0' bits were added before and after this data train respectively to simplify the boundary conditions. The electrical '1' bits were

raised-cosine shaped with a roll-off coefficient of 0.4 and were simulated using 40 samples per bit. The extinction ratio (ER) of the modulated OOK signal was set to be 12dB.

The signal was launched into an erbium-doped fibre amplifier (EDFA) amplified transmission link with 80km SMF per span and 0dBm signal launch power. The SMF was assumed to have CD of 16ps/km/nm, a nonlinear coefficient of 1.2/km/W, and a fibre loss of 0.2dB/km. Split-step Fourier method was used to calculate the signal propagation in the fibres and the step length was 1km at 0dBm signal launch power. At the end of each span, amplified spontaneous emission (ASE) noise from optical amplifiers was modelled as complex additive white Gaussian noise with zero mean and a power spectral density of $n_{sp}h\nu(G\text{-}1)$ for each polarization, where G and $h\nu$ are the amplifier gain and the photon energy respectively. n_{sp} is the population inversion factor of the optical amplifiers and was set to give a 4dB noise figure (NF).

The noise of the optical preamplifier was modelled as an additive white Gaussian noise for each polarization state. The launch power into the preamplifier was adjusted to control the OSNR. The pre-amplified signal was filtered by an 8.5GHz Gaussian-shaped optical band-pass filter (OBPF) which helped to suppress the optical noise and CD [4]. The signal after the OBPF was then split into two paths to extract $V_x(t)$ and $V_y(t)$, as shown in Fig. 2. The AMZI for the extraction of $V_y(t)$ had a $\pi/2$ differential phase shift and DTD of either 30ps or 10ps. The responsivities of the balanced detector and the direct detector were assumed to be 0.6A/W and 0.9A/W respectively, and equivalent thermal noise spectral power densities were assumed to be 100pA/Hz$^{1/2}$ and 18pA/Hz$^{1/2}$ respectively. These receiver parameters matched typical values of the commercial detectors used in the experimental demonstration in Section IV. The received powers of the detectors were 0dBm, unless otherwise specified. After detection, the signals were electrically amplified, filtered by 15GHz 4th-order Bessel electrical filters (EFs), and down-sampled to 50Gsamples/s to simulate the sampling effect of the real-time oscilloscope. The down-sampled copy of $V_x(t)$ was re-biased, which can significantly enhance the robustness of the scheme to thermal noise [13-14]. The amplitude of $V_y(t)$ was adjusted to correct for any gain imbalance of the $V_x(t)$ and $V_y(t)$ paths. Additional signal processing stages included a phase compensator to enhance the tolerance to differential phase misalignment of the AMZI [14] and a Gaussian-shaped high-pass EF to suppress the impairment from low-frequency amplification [15]. The full-field MLSE module, which was described in Fig. 1, operated with two samples per bit, 5-bit ADC resolution, and memory length m of 2 or 4 (corresponding to the state number of 4 and 16 respectively). For comparison, conventional DD MLSE and full-field FFE were also simulated, with the same quantization resolution and sampling number per bit as those in full-field MLSE. Mean-square-error (MSE) criterion was used to train and update the coefficients of full-field FFE.

The simulation was iterated ten times with different random number seeds to give a total of 184,230 simulated bits. The performance was evaluated in terms of the required optical signal-to-noise ratio (OSNR) to achieve a bit error rate (BER) of 5×10^{-4} by direct error counting. 184,230 bits were sufficient to produce a confidence interval of [3.5×10^{-4} 7×10^{-4}] for this BER with 99% certainty [16].

Fig. 3 shows the required OSNR versus fibre length by using conventional direct-detection MLSE (circles), full-field MLSE without a high-pass filter (triangles), and with a 1.25GHz high-pass filter in the phase estimation path for suppressing the amplification of low-frequency components (squares). The full metric (2) and a DTD of 30ps were employed for Fig. 3, where it was found that the full-field MLSE, without the proper suppression of low-frequency amplification, performed worse than conventional DD MLSE regardless of the memory length m. By optimizing the low-frequency response for the estimated frequency (squares), phase estimation was significantly improved. This strongly suggests that full-field MLSE can significantly outperform DD MLSE for both 4 and 16 states. At a OSNR of 15 dB (~ 5dB penalty with respect to back-to-back sensitivity), the CD tolerance was enhanced from 270km to 420km, and from 400km to 580km for m of 2 and 4 respectively, representing approximately 50% performance improvement.

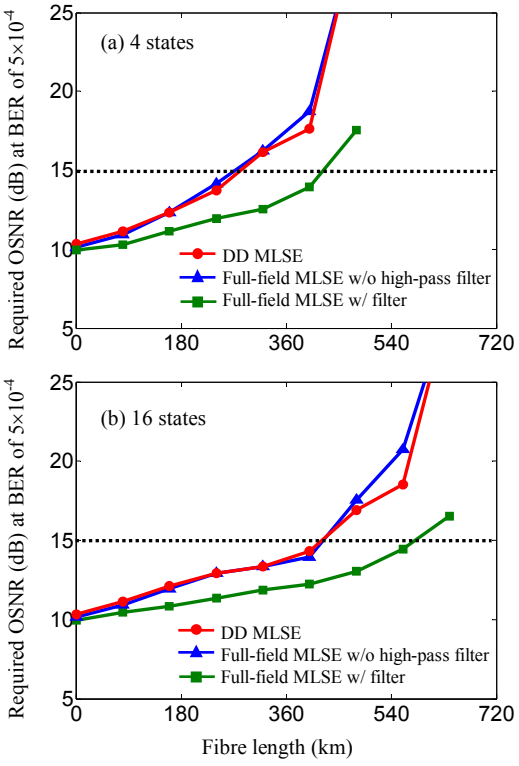

Fig. 3. Required OSNR versus transmission reach when the MLSE memory length is (a) 2 and (b) 4. The DTD of the AMZI is 30ps.

Fig. 3 depicts the system performance obtained under near-optimum parameter values. In practice, it would be essential to understand the performance sensitivity to system parameters and consequently develop important design criteria.

Although the system operates in the ASE-limited operating regime, receiver thermal noise can also play an important role in the performance of the EDC scheme. This is because the

received power of the instantaneous frequency, $V_y(t)$, is linearly proportional to the DTD of the AMZI:

$$V_y(t) \propto |E(t)|^2 \Delta\omega(t)\Delta t + n_{th\_y} \tag{4}$$

where n_{th_y} is the thermal noise on $V_y(t)$. For small DTD, it is clear from (4) that the power level of $V_y(t)$ can be very small even for high received signal power $|E(t)|^2$. The DTD must therefore be properly designed to a balance between values favouring linear estimation of $V_y(t)$ and thermal noise. Another effect of signal-independent thermal noise arises from the effect of denominator that represents the total received signal power used in the phase estimation:

$$V_x(t) \propto |E(t)|^2 + n_{th\_x}$$
$$V_f(t) \propto \frac{\alpha V_y(t)}{(V_x(t) + bias)} = \frac{|E(t)|^2 \Delta\omega(t) + n_{th\_y}/\Delta t}{2\pi(|E(t)|^2 + bias + n_{th\_x})} \tag{5}$$

where α and *bias* are a scaling factor and the bias added to $V_x(t)$ (see Fig. 2). n_{th_x} is the thermal noise on $V_x(t)$. It is apparent that thermal noise has much more impact on the accuracy of the $V_f(t)$ estimation for a logical data '0' than for a logical data '1'. This is in marked contrast to the impact of signal-spontaneous beat noise, where the influence of the denominator is mitigated by the reduced signal dependent noise for a logical data '0'. In (5), we also include a DC bias, often necessary to accommodate AC coupling of the receiver chain. In addition, the DC bias may increase the value of the denominator, which for sequences of consecutive logical data '0's, would reduce the impact of thermal noise albeit at the expense of a slight distortion in the reconstructed frequency. The effect of the DC bias on the required OSNR is shown in Fig. 4, where we plot the required OSNR as a function of excess DC bias (over that required to cancel the effects of AC coupling). A modest increase in bias of 10% appears sufficient to mitigate the effect of division by small values for sequences of consecutive logical data '0's.

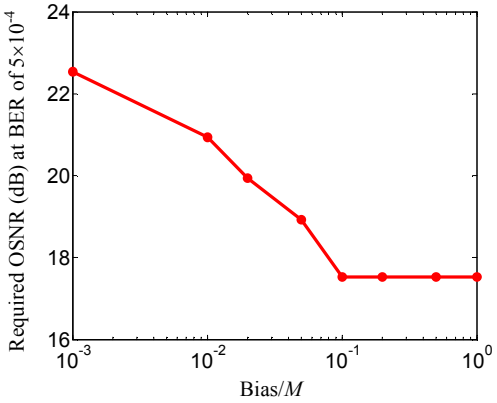

Fig. 4. Required OSNR versus normalized bias added to the intensity signal $V_x(t)$ at a system length of 480km using 4-state full-field MLSE with metric (2). The AMZI DTD is 30ps. M represents the average detected signal amplitude ($[E\{|V_x(t)|^2\}]^{1/2}$) and $E\{\cdot\}$ represents the ensemble average.

DTD also impacts the accuracy of the frequency reconstruction. Fig. 5 depicts the required OSNR as a function of the power entering the photodiodes for different AMZI DTD and DC bias values. A received optical power larger than 9dBm was required to minimise the penalty from the thermal noise for a 10ps AMZI DTD and 0V bias. This strict requirement was relaxed to around 5dBm by either using a AMZI with a larger DTD or properly biasing $V_x(t)$. By both biasing $V_x(t)$ and using an AMZI with a 30ps DTD (squares), negligible OSNR penalty was observed at 0dBm received optical power. This greatly relaxed the requirements for the gain of the optical preamplifier, the loss of the OBPF and the AMZI, and the power handling of the detectors.

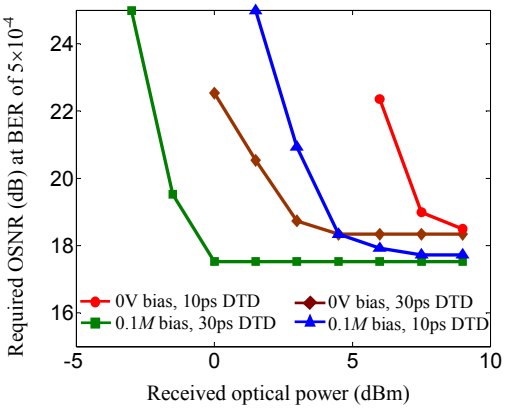

Fig. 5. Required OSNR versus received optical power at a system length of 480km using 4-state full-field MLSE (m=2).

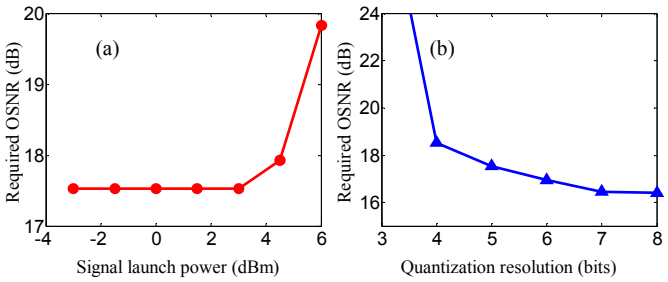

Fig. 6. Required OSNR at BER of 5×10^{-4} versus (a) the signal launch power per span and (b) the ADC resolution at 480km using 4-state full-field MLSE with metric (2).

The effect of optical fibre nonlinearities was also investigated, as shown in Fig. 6(a), which depicts the required OSNR versus the signal launch power at 480km using 4-state full-field MLSE. The lookup table was trained for each power level. The step length in the split-step Fourier method was also adjusted to ensure the calculation accuracy (smaller step length for higher signal launch power). We found that fibre nonlinearities induced a negligible penalty on the system performance if the signal launch power was less than 3dBm, which was the case used in the experiments in Section IV.

In electronic signal processing, ADC resolution is always a balance between the performance and electronic complexity. Fig. 6(b) depicts the performance as a function of quantization resolution where it is clear that the 5-bit resolution used in the simulation resulted in around ~1dB penalty when compared to the 8-bit reference. This is achievable using modern microelectronic technologies where the state-of-the-art ADCs can have a resolution of 6~8 bit at 30~56Gsamples/s.

As discussed above, the full metric (2) can be approximated by computing the two marginal probabilities instead of a single

joint probability. Fig. 7 compares the required OSNR obtained using this reduced metric (3) (circles) and the full metric (2) (triangles) when the memory length m is (a) 2 and (b) 4. Solid and dashed lines represent the cases with and without a 1.25GHz high-pass filter. The figures clearly show that the high-pass filter was critical for the optimum operation of full-field MLSE using metric (3). This is because when the system was dominated by low-frequency component amplification, a correlation in the noise statistics of the extracted real and imaginary components might be expected, so breaking the assumption leading to (3). In contrast, optimization of the low-frequency response enabled metric (3) to exhibit similar compensation performance to that using metric (2), with the advantage of a significant reduction in the complexity.

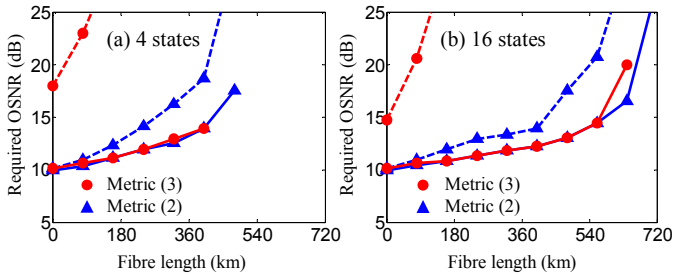

Fig. 7. Required OSNR at BER of 5×10^{-4} as a function of transmission reach using metric (2) (triangles) and metric (3) (circles) without (dashed) and with (solid) a high-pass filter.

To further identify the applications of full-field MLSE for optical communications, we compare the performance of full-field MLSE and full-field FFE in Fig. 8 under (a) optimized system parameters as discussed above, and (b) non-optimized parameters resulting in not fully suppressed noise and noise amplifications in full-field reconstruction. The parameters for (b) closely match those used in the experiments in Section IV. It is clearly seen that when the noise and its amplification mechanisms were suppressed (Fig. 8(a)), 16-state (m=4) full-field MLSE exhibited better performance compared to full-field FFE with the same memory length, but had less compensation distance when compared to full-field FFE with m=8 and 16. Increasing the memory length of full-field MLSE can overcome this limitation but would increase the complexity exponentially, hindering its applications for longer-distance transmissions. However, for dispersion compensating fibre (DCF) free metropolitan area networks with transmission reach around several hundred kilometers, full-field MLSE is a more effective approach. The reason is threefold. Firstly, it requires low implementation complexity for small m values (≤4), which is achievable by modern microelectronic technologies. Secondly, it exhibits better performance limit than that of full-field FFE with the same m [1]. Finally, full-field MLSE has much better tolerance to the noise and the associated noise amplification mechanisms in full-field reconstruction. Fig. 8(b) shows that when the system parameters were not fully optimized, the performance of full-field FFE was degraded severely, and was poorer than that of 16-state full-field MLSE even when m increased to 16. Consequently, stringent limit on the design of system parameters should be placed on full-field FFE, but it can be greatly relaxed by full-field MLSE.

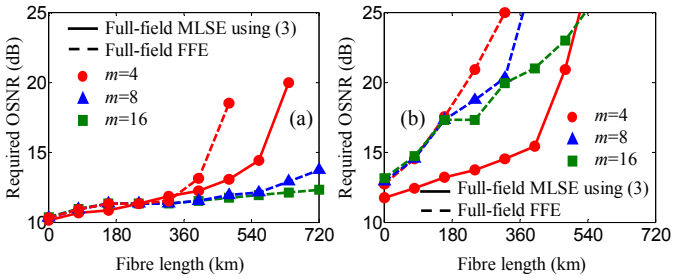

Fig. 8. Required OSNR versus fibre length by using metric (3) based full-field MLSE with memory length m of 4 (solid circles), and full-field FFE (dashed) with m of 4 (circles), 8 (triangles), and 16 (squares). (a): 8.5GHz OBPF, AMZI with 30ps DTD, and 0dBm received power of the photodiodes; (b): 0.8nm OBPF, AMZI with 10ps DTD, and -3dBm received power. In (a)-(b), the high-pass filter bandwidth and the bias added to $V_x(t)$ are optimized.

IV. Experimental Verification

Fig. 9 shows the setup of the system used for experimental verification of our simulations. A 1557nm signal from a distributed feedback (DFB) laser was intensity modulated using a MZM giving a 12dB ER signal at 10Gbit/s with a 2^{11}-1 PRBS data. The generated OOK signal was transmitted over a recirculating loop comprising 124km of BT Ireland's field-installed SMF between Cork City and Clonakilty, County Cork, Ireland, with a signal launch power of around 0dBm per span. At this launch power, fibre nonlinear effects, as we showed in Section III, were expected to be negligible. The noise figure of the loop amplifiers was 4.5dB. The signal polarisation was randomised after each recirculation using an Adaptif A3200-1 synchronous polarisation scrambler. Although not explicitly depicted in Fig. 9, a 3nm-wide band (1550-1553nm) of ASE noise, with spectral power density 20dB less than that of the signal, co-propagated with the signal to ensure that the loop amplifier was appropriately saturated. The ASE noise was obtained from an EDFA filtered by an eight-channel arrayed waveguide.

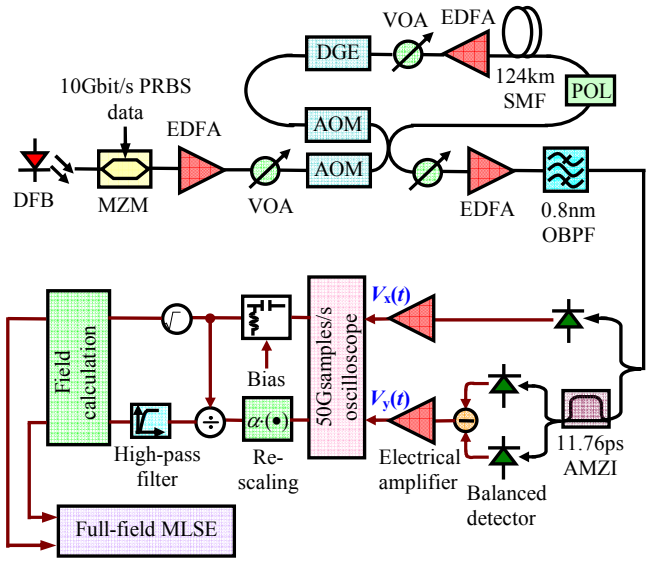

Fig. 9. Experimental setup (AOM: Acousto-optic modulator; DGE: Dynamic gain equaliser; VOA: Variable optical attenuator)

At the receiver, the signal was pre-amplified and optically filtered by a 0.8nm OBPF. The optical attenuator before the

preamplifier was adjusted to obtain varied OSNR values. Ten percent of the signal power was directly detected by a 10Gbit/s receiver and electrically amplified by a 12GHz electrical amplifier. The remaining signal was optically processed by an AMZI with a 11.76ps DTD (85GHz free spectral range) and π/2 differential phase shift, detected by a 40GHz balanced detector, and electrically amplified with a net amplification bandwidth of 15GHz. The use of 40GHz balanced detector for 10Gbit/s signal detection was restricted by our equipment availability, and the bandwidth of this path was limited by the following electrical amplifiers. Both detected signals, represented by $V_x(t)$ and $V_y(t)$, were sampled by a real-time oscilloscope at 50Gsamples/s with 8-bit resolution. Off-line processing with 5,000,000 samples per channel (1,000,000 bits) was used for optical intensity and phase recovery. $V_x(t)$ was re-biased to allow for the AC coupling of the receiver and to enhance the robustness to thermal noise as discussed above. $V_y(t)$ was re-scaled to correct for different gains of the $V_x(t)$ and $V_y(t)$ signal paths. A Gaussian-shaped high-pass filter with 1GHz 3dB bandwidth was placed in the frequency estimation path to improve the quality of phase estimation and accordingly the compensation performance. In the case of DD MLSE, only V_x(t) was used. MLSE re-quantized the signals with 5-bit resolution and operated at two samples per bit, unless otherwise specified. Full-field FFE used MSE criterion for coefficient training and update.

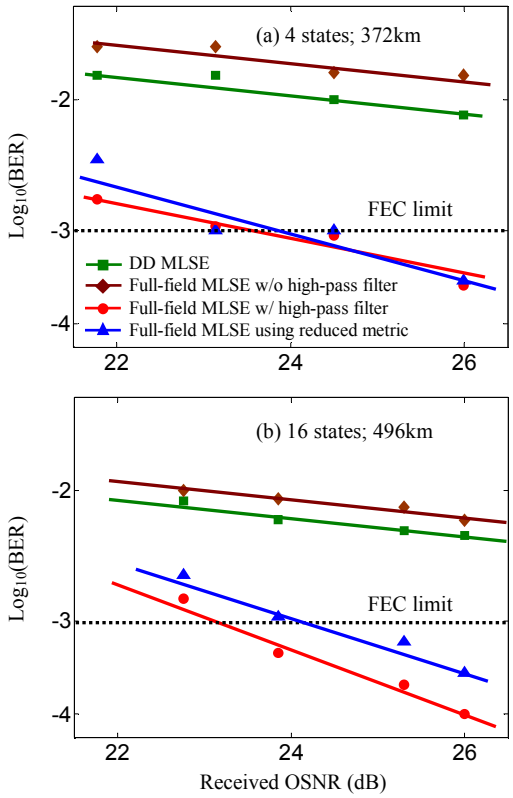

Fig. 10. Performance versus received OSNR for (a) 372km transmission using 4-state MLSE and (b) 496km transmission using 16-state MLSE. Squares, diamonds, and circles represent DD MLSE, full-field MLSE without and with a high-pass filter respectively. The full metric (2) is used for full-field MLSE. Triangles represent full-field MLSE using the reduced metric (3) under optimized high-pass filter bandwidth.

Fig. 10 depicts $1\log_{10}$(BER) versus received OSNR following transmission over (a) 372km and (b) 496km of field-installed SMF using 4 state and 16 state MLSE respectively. It is confirmed by the figure that full-field MLSE without a high-pass filter (diamonds) exhibited even worse performance compared to DD MLSE (squares), and adequate transmission performance was unachievable (BER was always above the FEC limit of 10^{-3}) in both cases. By proper suppressing low-frequency amplification using a high-pass filter (circles), a significant performance improvement was observed, and full-field MLSE enabled a BER of 2.8×10^{-4} and 1×10^{-4} to be recorded for 372km at 4 states and 496km at 16 states respectively, confirming the effectiveness of the technique.

To investigate the performance of metric (3) with reduced complexity, Fig. 10 also compares $\log_{10}$(BER) versus received OSNR using full-field MLSE based on full metric (2) (circles), and the reduced metric (3) (triangles). It can be seen that the reduced metric exhibited negligible performance degradation at 372km and 4 states despite significantly reduced complexity of the lookup table. For 496km and 16 states, a small penalty was observed, but it was not severe and full-field MLSE using metric (3) should still enable a BER of 3×10^{-4} at 26dB OSNR.

It should be noted that the experimental parameters were not fully optimized due to the device availability, including for example 11.76ps AMZI and insufficient gain of the pre-amplifier resulting in less robustness to thermal noise. We verified the performance advantage of full-field MLSE compared to the combination of full-field detection and other EDC methods under non-optimized system parameters. Fig. 11 depicts $\log_{10}$(BER) versus received OSNR at 496km by using 16-state full-field MLSE with the reduced metric (3) (circles), full-field FFE (triangles and squares), and full-field EDC based on a dispersive transmission line (diamonds) [14]. It is observed that full-field EDC using a dispersive transmission line and full-field FFE with m=8 could not achieve 496km transmission (BER>10^{-3}). Increasing m of full-field FFE to 16 enabled a better BER below 10^{-3} at 26dB OSNR, but its performance was still poorer than that of full-field MLSE with m=4, verifying the theoretical prediction in Fig. 8(b).

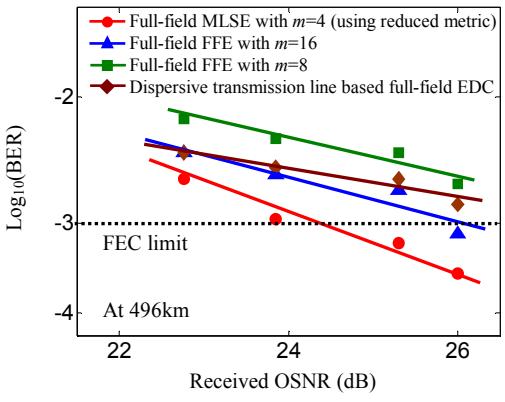

Fig. 11. Log_{10}(BER) versus received OSNR at 496km. Circles, triangles, squares, and diamonds represent 16-state (m=4) full-field MLSE using reduced metric (3), full-field FFE with memory length of 16 (triangles) and 8 (squares), and full-field EDC based on a dispersive transmission line respectively. High-pass filter bandwidth was optimized.

The impact of the high-pass filter on the performance of full-field MLSE was further investigated in Fig. 12(a), which illustrates the variation in $\log_{10}$(BER) at 26dB OSNR and 372km versus the filter bandwidth. We observed that when the low-frequency component amplification was suppressed (above 0.6GHz bandwidth), the metric (3) and (2) performed equally well (BER<10^{-3}). However, when the system was dominated by low-frequency component amplification, the performance of the reduced metric (3) was degraded more severely, matching the theoretical prediction in Fig. 7.

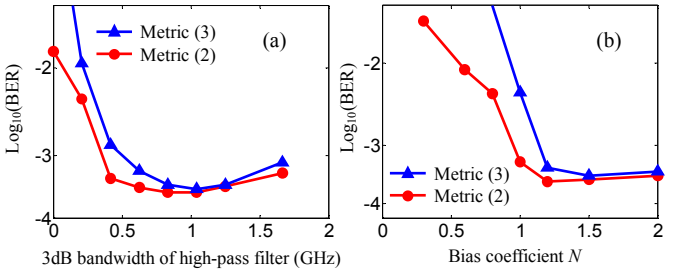

Fig. 12. Performance versus (a) 3dB bandwidth of high-pass filter and (b) bias coefficient N using 4-state full-field MLSE with metric (2) (circles) and metric (3) (triangles) after 372km transmission.

The performance sensitivity to the bias coefficient was shown in Fig. 12(b). Note that due to AC coupling of the receivers, the absolute bias value added to the signal intensity $V_x(t)$ here was different from that used in the simulations (Fig. 4), and was calculated to be $-N\cdot\min(V_x(t))$, where $\min(V_x(t))$ had a negative value. From Fig. 12, it may be seen that it was essential to bias the sampled values of $V_x(t)$ to a value larger than zero (N>1) for proper operation of full-field MLSE. This is because $V_f(t)=V_y(t)/(V_x(t)+bias)$ had an instantaneous π phase shifts whenever $V_x(t)+bias$ changed sign. When the noise amplification due to the denominator, $V_x(t)+bias$, was suppressed (N>1), the system performance was robust to further bias increase, matching the numerical results in Fig. 4.

Finally, the $\log_{10}$(BER) versus the complexity of the lookup table, and the length of the training sequence are depicted in Fig. 13 and 14 respectively. The lookup table sizes of DD MLSE, full-field MLSE using full metric and reduced metric were proportional to 2^{q+m+2}, 2^{2q+m+2}, and 2^{q+m+3} respectively. The variation of x axis in Fig. 13 was attained by adjusting the ADC resolution. It can be appreciated that for all curves, the BER was reduced as the complexity or the length of training sequence increased, and DD MLSE exhibited the least complexity. However, the full-field MLSE method showed greatly improved maximum achievable performance compared to the DD MLSE technique. The comparison between metric (2) and metric (3) showed that the minimum required memory size and training sequence length for the metric (3) to achieve BER of 1×10^{-3} were reduced by around one order of magnitude compared to the metric (2), confirming its benefit in complexity reduction. Note that in Fig. 14, the histogram method was used. By using parametric method for channel estimation, the required length of training sequence can be further reduced.

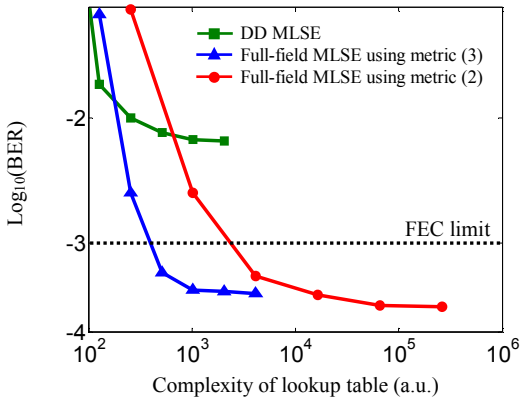

Fig. 13. Log_{10}(BER) versus complexity of lookup table (required memory and an associated searching time) at 372km and 26dB OSNR using 4-state MLSE. The length of training sequence is 500,000 bits and the 3dB bandwidth of high-pass filter is 1GHz.

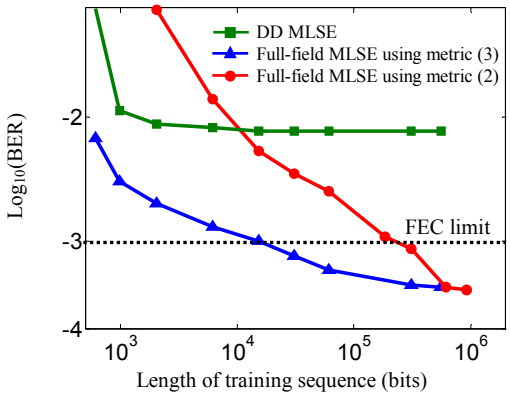

Fig. 14. Log_{10}(BER) versus the length of training sequence at 372km and 26dB OSNR using 4-state MLSE. The ADC resolution is 5 bits and the bandwidth of the high-pass filter is 1GHz.

V. Conclusion

We have systematically investigated full-field MLSE for CD compensation in 10Gbit/s OOK based optical transmissions in both simulations and experiments. Important design criteria, including suppression of low-frequency amplification, intensity bias, ADC resolution, and fibre nonlinearity have been identified. This paper confirms the performance benefits of full-field MLSE compared to DD MLSE at both 4 and 16 states, without significantly increasing the electronic computation complexity. It is also verified that full-field MLSE is more robust to the noise and the associated noise amplification mechanisms in full-field reconstruction and can greatly relax the specifications of system components when compared to full-field EDC using FFE or a dispersive transmission line. These performance and design benefits increase the potential of full-field MLSE for DCF free metropolitan area networks.

Acknowledgment

The authors gratefully acknowledge BT Ireland, particularly J.Coleman, M.Conroy, W.McAuliffe, R.O'Regan and M.O'Reilly, for providing access to the optical fibre link.

REFERENCES

[1]. J.G. Proakis, *Digital Communications*, 4th Edition, McGraw-Hill, 2001.

[2]. P. Poggiolini, and G. Bosco, "Long-haul WDM IMDD transmission at 10.7Gbit/s in a dispersion-managed multispan system using MLSE receivers," *IEEE J. Lightw. Technol.*, vol. 26, pp. 3041-3047, 2008.

[3]. J. Zhao, L.K. Chen, "Three-chip DPSK maximum likelihood sequence estimation for chromatic-dispersion and polarization-mode-dispersion compensation", *Opt. Lett.*, vol. 32, pp. 1746-1748, 2007.

[4]. C. Xia, W. Rosenkranz, "Electrical dispersion compensation for different modulation formats with optical filtering," *Optical Fibre Communication Conference* (OFC), paper OWR2, 2006.

[5]. S. Chandrasekhar, A.H. Gnauck, G. Raybon, L.L. Buhl, D. Mahgerefteh, X. Zheng, Y. Matsui, K. McCallion, Z. Fan, and P. Tayebati, "Chirp-managed laser and MLSE-RX enables transmission over 1200km at 1550nm in a DWDM environment in NZDSF at 10Gb/s without any optical dispersion compensation," *IEEE Photon. Technol. Lett.*, vol. 18, pp. 1560-1562, 2006.

[6]. T. Ellermeyer, J. Mullrich, J. Rupeter, H. Langenhagen, A. Bielik, and M. Moller, "DA and AD converters for 25 GS/s and above," *IEEE/LEOS Summer Topical Meetings,* pp. 117-118, 2008.

[7]. A. Farbert, S. Langenbach, N. Stojanovic, C. Dorschky, T. Kupfer, C. Schulien, J.-P. Elbers, H. Wernz, H. Griesser, and C. Glingener, "Performance of a 10.7 Gb/s receiver with digital equaliser using maximum likelihood sequence estimation,", *European Conference on Optical Communication* (2004), PDP Th4.1.5.

[8]. M. Alfiad, D. van den Borne, A. Napoli, A.M.J. Koonen, and H.De Waardt, "A DPSK receiver with enhanced CD tolerance through optimized demodulation and MLSE," *IEEE Photon. Technol. Lett.*, vol. 20, pp. 818-820, 2008.

[9]. J.M. Gene, P.J. Winzer, R.J. Essiambre, S. Chandrasekhar, Y. Painchaud, and M. Guy, "Experimental study of MLSE receivers in the presence of narrowband and vestigial sideband optical filtering," *IEEE Photon. Technol. Lett.*, vol. 19, pp. 1224-1227, 2007.

[10]. Y. Cai, "Coherent detection in long-haul transmission systems," in *Proc. Optical Fibre Communication Conference* (OFC), OTuM1, 2008.

[11]. Ivan P. Kaminow, T. Li, A.E. Willner, *Optical Fiber Telecommunications V B*, 5th Edition, Elsevier, 2008.

[12]. A.D. Ellis and M.E. McCarthy, "Receiver-side electronic dispersion compensation using passive optical field detection for low cost 10Gbit/s 600 km-reach applications," in *Proc. Optical Fibre Communication Conference* (2006), paper OTuE4.

[13]. M.E. McCarthy, J. Zhao, P. Gunning, and A.D. Ellis, "A novel field-detection maximum-likelihood sequence estimation for chromatic dispersion compensation," *European Conference on Optical Communications* (ECOC), paper We.2.E.5, Brussels, Belgium, 2008.

[14]. J. Zhao, M.E. McCarthy, and A.D. Ellis, "Electronic dispersion compensation using full optical-field reconstruction in 10Gbit/s OOK based systems," *Opt. Express*, vol. 16, pp. 15353-15365, 2008.

[15]. J. Zhao, M.E. McCarthy, P. Gunning, and A.D. Ellis, "Chromatic dispersion compensation using full optical-field maximum likelihood sequence estimation," *Optical Fibre Communication Conference* (OFC), paper OThE6, 2009.

[16]. M. Jeruchim, "Techniques for Estimating the Bit Error Rate in the Simulation of Digital Communication Systems," *IEEE J. Selected Areas in Communications,* vol. 2, pp. 153-170, 1984.

Dr Jian Zhao received a B.Eng degree from University of Science and Technology of China (USTC) in 2002, M.Phil. and Ph.D. degrees from the Chinese University of Hong Kong (CUHK) in 2004 and 2007 respectively. He joined the Photonic Systems Group at the Tyndall National Institute as a Postdoctoral Research Scientist in August 2007. His current research interests include electronic signal processing in optical communications and spectrally-efficient multi-carrier optical transmission systems.

Dr Zhao is a member of IEEE and is an Enterprise Ireland principal investigator. He was the recipient of the First Prize of Outstanding Student Scholarship of USTC. He has published more than 30 technical papers in peer-reviewed international journals and conferences and 2 patents.

Mary McCarthy was born in Mallow, Ireland in 1984 and gained a B.Eng in Electrical and Electronic Engineering from University College Cork, Cork, Ireland in 2004.

She is currently with the Photonic Systems Group at the Tyndall National Institute in Cork, Ireland where her research interests include the application of electronic signal processing to optical communication systems.

Dr. Andrew Ellis was born in Underwood, England in 1965 and gained a BSc in Physics with a minor in mathematics from the University of Sussex, Brighton, England in 1987. He was awarded his PhD in Electronic and Electrical Engineering from The University of Aston in Birmingham, Birmingham, England in 1997 for his study on All Optical Networking Beyond 10Gbit/s.

He previously worked for British Telecom Research Laboratories as a Senior Research Engineer investigating the use of optical amplifiers and advanced modulation formats in optical networks and the Corning Research Centre as a Senior Research Fellow where he led activities in optical component characterisation. Currently, he heads the Transmission and Sensors Group at the Tyndall National Institute in Cork, Ireland, where he is also a member of the Department of Physics, University College Cork. He research interests include the evolution of core and metro networks, and the application of photonics to sensing.

Dr Ellis is a member of the Institute of Physics and the Institute of Engineering Technology, and is a Chartered Physicist. He acts as a reviewer for IEEE Journal of Lightwave Technology and Photonics Technology Letters and has published over 100 journal papers and over 20 patents in the field of Photonics.

Dr. Paul Gunning joined BT Laboratories in 1994 to investigate high-speed all-optical networks and photonic packet switching. In 1998 he moved to BT's Futures Testbed where he works on Ethernet, router performance testing, Layer 2/Layer 3 MPLS VPNs and reconfigurable optical networks. Paul graduated with a B.Sc. in Applied Physics from Dublin City University in 1992. He was awarded an M.Sc. in laser physics and a Ph.D in photonic switching networks from Essex University in 1995 and 2001 respectively.